Article

Neuron

Bcl11a (Ctip1) Controls Migration of Cortical Projection Neurons through Regulation of *Sema3c*

Highlights

- Bcl11a controls cell polarity and radial migration of upper layer cortical neurons
- Sema3c is a major downstream effector of Bcl11a in migrating cortical neurons
- Morphogenesis and survival of postmigratory upper layer neurons depend on Bcl11a
- Deletion of Bcl11a in mice results in hypoplasia of superficial neocortex

Authors

Christoph Wiegreffe, Ruth Simon, Katharina Peschkes, ..., Neal G. Copeland, Victor Tarabykin, Stefan Britsch

Correspondence

stefan.britsch@uni-ulm.de

In Brief

Wiegreffe et al. discover a novel Bcl11a/Sema3c-dependent regulatory pathway that controls polarization and radial migration of late-born upper layer cortical projection neurons. Deletion of Bcl11a in mice ultimately results in severe hypoplasia of upper neocortical layers.

Accession Numbers

GSE52827

Wiegreffe et al., 2015, Neuron *87*, 311–325
July 15, 2015
http://dx.doi.org/10.1016/j.neuron.2015.06.023

CellPress

Neuron
Article

Bcl11a (Ctip1) Controls Migration of Cortical Projection Neurons through Regulation of *Sema3c*

Christoph Wiegreffe,[1] Ruth Simon,[1] Katharina Peschkes,[1] Carolin Kling,[1] Michael Strehle,[2] Jin Cheng,[1,7] Swathi Srivatsa,[3] Pentao Liu,[4] Nancy A. Jenkins,[5] Neal G. Copeland,[5] Victor Tarabykin,[3,6] and Stefan Britsch[1,*]
[1]Institute of Molecular and Cellular Anatomy, Ulm University, Albert-Einstein-Allee 11, 89081 Ulm, Germany
[2]Max Delbrück Center for Molecular Medicine, Robert-Rössle-Strasse 10, 13125 Berlin, Germany
[3]Institute of Cell Biology and Neurobiology, Center for Anatomy, Charité-Universitätsmedizin Berlin, Virchowweg 6, 10117 Berlin, Germany
[4]Wellcome Trust Sanger Institute, Hinxton, Cambridge CB10 1HH, UK
[5]The Methodist Hospital Research Institute, 6670 Bertner Avenue, Houston, TX 77030, USA
[6]Institute of Biology and Biomedicine, Lobachevsky State University of Nizhny Novgorod, 23 Prospekt Gagarina (Gagarin Avenue), 603950 Nizhny Novgorod, Russia
[7]Present address: Institute of Microscopic Anatomy and Neurobiology, University Medical Center, Johannes Gutenberg University, Langenbeckstrasse 1, 55131 Mainz, Germany
*Correspondence: stefan.britsch@uni-ulm.de
http://dx.doi.org/10.1016/j.neuron.2015.06.023

SUMMARY

During neocortical development, neurons undergo polarization, oriented migration, and layer-type-specific differentiation. The transcriptional programs underlying these processes are not completely understood. Here, we show that the transcription factor Bcl11a regulates polarity and migration of upper layer neurons. *Bcl11a*-deficient late-born neurons fail to correctly switch from multipolar to bipolar morphology, resulting in impaired radial migration. We show that the expression of *Sema3c* is increased in migrating *Bcl11a*-deficient neurons and that Bcl11a is a direct negative regulator of Sema3c transcription. In vivo gain-of-function and rescue experiments demonstrate that Sema3c is a major downstream effector of Bcl11a required for the cell polarity switch and for the migration of upper layer neurons. Our data uncover a novel Bcl11a/*Sema3c*-dependent regulatory pathway used by migrating cortical neurons.

INTRODUCTION

The neocortex plays a major role in cognitive, emotional, and sensory-motor functions. All parts of the neocortex have a common principle structure, with neurons organized in six horizontal layers, oriented parallel to the brain surface (Kwan et al., 2012). During development of the neocortex, progenitor cells located in the dorsal wall of the lateral ventricle give rise to immature projection neurons that migrate radially toward the pial surface and acquire a layer-specific neuronal identity. While early-born neurons populate the deep cortical layers, late-born neurons migrate past the deep cortical layers to settle in the upper cortical layers. After being generated in the ventricular and subventricular zones (VZ/SVZ), postmitotic neurons become transiently multipolar, slow their migration, and explore the environment for signals required for further development. After a short stay in the intermediate zone (IZ), prospective cortical projection neurons switch to a bipolar morphology, attach to the radial glial scaffold, and initiate radial migration into the cortical plate (CP) (LoTurco and Bai, 2006; Noctor et al., 2004; Tabata and Nakajima, 2003). Upon reaching their destined target layers cortical neurons detach from radial glial fibers and undergo layer type-specific terminal differentiation. Mutations affecting different steps of neuronal migration lead to severe cortical malformations, such as lissencephaly or white matter heterotopias (Evsyukova et al., 2013).

The migration of cortical projection neurons is regulated on several levels: (1) by genes such as *Lis1*, *Ndel1*, or *Dcx*, involved in the direct control of cell motility and the modulation of cytoskeletal dynamics, (2) by cell-type-specific transcriptional programs, and (3) by extracellular signals, providing instructive cues to migrating neurons (Evsyukova et al., 2013; Kwan et al., 2012). For example, the transcription factors Satb2, Pou3f2 (Brn2), and Pou3f3 (Brn1) are enriched in upper-layer cortical neurons, and their genetic ablation in mice results in aberrant specification and migration of late-born neurons (Alcamo et al., 2008; Britanova et al., 2008; Kwan et al., 2012; McEvilly et al., 2002; Sugitani et al., 2002). The signals acting downstream of transcriptional regulators that control cortical neuron migration are incompletely defined. Various members of class III semaphorins are present along the migratory route of cortical projection neurons, and their cognate receptors of the neuropilin and plexin families are expressed by migrating cortical neurons. Functional studies suggest that class III semaphorins provide guidance cues to migrating cortical neurons (Chen et al., 2008; Ito et al., 2008; Marín et al., 2001; Tamamaki et al., 2003).

Bcl11a (*Ctip1*) encodes a zinc-finger protein that regulates transcription through interaction with COUP-TF proteins, as well as direct, sequence-dependent DNA binding (Avram et al., 2002; John et al., 2012). We recently demonstrated that Bcl11a is essential for morphogenesis and wiring of projection neurons in the dorsal spinal cord (John et al., 2012). Bcl11a is also expressed in the developing murine neocortex (Leid et al., 2004).

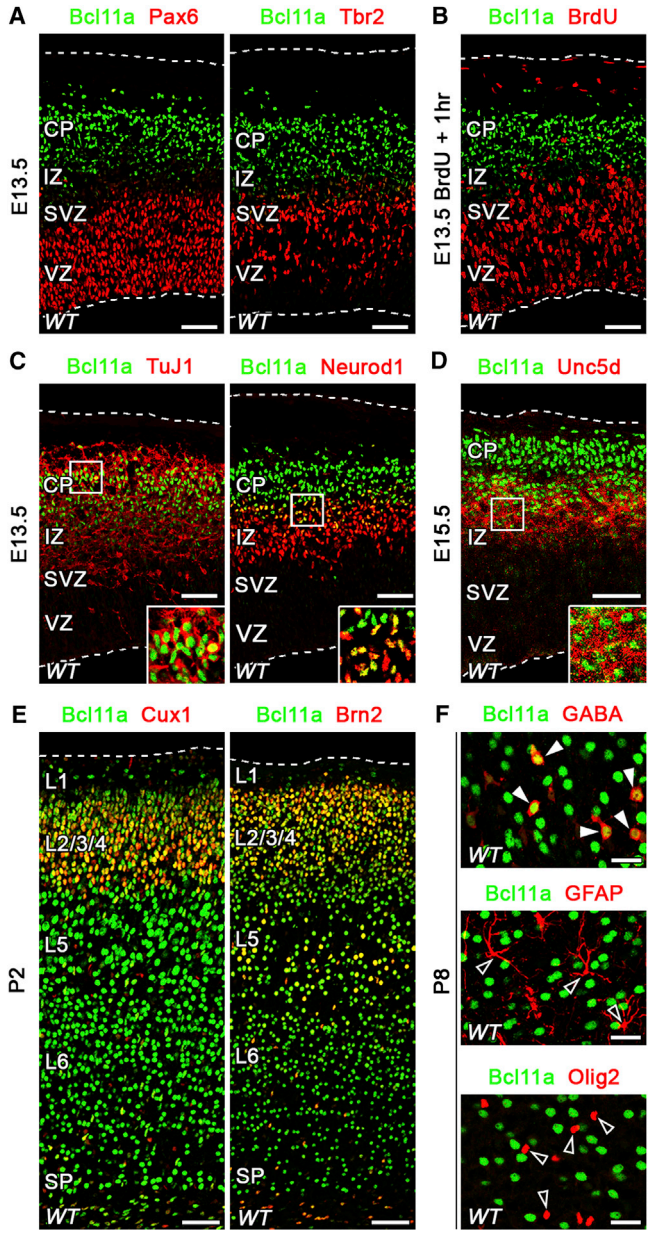

Figure 1. Bcl11a Is Expressed in Postmitotic Cortical Projection Neurons

(A) Bcl11a does not co-localize with Pax6 (left) or Tbr2 (right) expression in the ventricular and subventricular zones (VZ/SVZ) in E13.5 wild-type (WT) neocortex.

(B) Injection of BrdU at E13.5 1 hr before brain dissection does not show BrdU incorporation into Bcl11a-positive cells.

(C and D) Co-staining of Bcl11a with TuJ1 (C, left) and Neurod1 (C, right) at E13.5 or Unc5d (D) at E15.5 showing co-localization in the cortical plate (CP) and intermediate zone (IZ). The insets represent enlargements of the boxed areas.

(E) Bcl11a-positive cells co-express Cux1 (left) and Brn2 (right) in P2 neocortex. Cortical layers L1–L6 are indicated. SP, subplate.

(F) Co-staining for Bcl11a and lineage-specific markers (GABA, GFAP, and Olig2) showing expression of Bcl11a in interneurons, but not in glial cells, at P8. Filled arrowheads point at Bcl11a-positive cells co-expressing GABA. Open arrowheads point at GFAP- or Olig2-positive cells that do not express Bcl11a. Scale bars, 50 μm (A–E) and 25 μm (F). See also Figures S1 and S2.

Several studies in humans strongly suggest that *BCL11a* is a candidate gene for the 2p15-16.1 microdeletion syndrome, which is associated with neocortical dysplasia and mental retardation (Basak et al., 2015; Hancarova et al., 2013; Peter et al., 2014; Rajcan-Separovic et al., 2007). Here, we provide evidence that Bcl11a is essential for neocortical development. *Bcl11a* mutant late-born cortical neurons are impaired to switch from multipolar to bipolar morphology and fail to migrate, resulting in delayed arrival at their final destination. Postmigratory neocortical neurons require early, but not late, expression of Bcl11a for their morphogenesis and survival. Finally, we identify *Sema3c* as a direct Bcl11a target gene that controls cortical projection neuron polarization and migration. Taken together, in this study, we identify a novel Bcl11a/*Sema3c*-dependent regulatory pathway controlling migration of cortical projection neurons.

RESULTS

Bcl11a Is Expressed in Young Neocortical Neurons

During cortex development, Bcl11a protein expression is restricted to projection neurons and some GABAergic interneurons, but is excluded from proliferating progenitors of the VZ/SVZ or from glia (Figures 1A, 1B, and 1F). At postnatal day 2 (P2), at which time most migrating cortical projection neurons reached their designated layers, we noted that Bcl11a protein expression overlaps with the expression of Cux1 (Nieto et al., 2004) and Brn2 (McEvilly et al., 2002; Sugitani et al., 2002), both identifying late-born upper-layer projection neuron populations (Figure 1E). At P2, Bcl11a expression was also detected in Brn2/Cux1-negative deep-layer neurons (Figure 1E). Between E13.5 and 15.5, during which time migrating cortical neurons leave the Unc5d and Neurod1-positive SVZ/IZ (Mattar et al., 2008; Sasaki et al., 2008), we found co-localization of both markers with Bcl11a, most prominently in the upper IZ (Figures 1C and 1D).

Late-Born Cortical Neurons Require Bcl11a for Migration

To study the functions of Bcl11a in cortical development, we generated a conditional mouse model. Homozygous recombination of a $Bcl11a^{flox}$ allele (John et al., 2012) in either cortical progenitor cells ($Bcl11a|Emx1^{Cre}$ mutant) or postmitotic projection neurons ($Bcl11a|Nex^{Cre}$ mutant) resulted in effective ablation of Bcl11a protein (Figures S1A and S1B). Bcl11a ablation caused a marked reduction of cortical thickness and layer disorganization, while at P2 the total number of neurons remained unchanged (Figures S1C–S1F). Next, we analyzed the proliferation and survival of $Bcl11a|Emx1^{Cre}$ mutant neurons. At E14.5 and E16.5, the number of proliferating progenitor cells, as identified by incorporation of bromodeoxyuridine (BrdU), and the simultaneous expression of Pax6 and Tbr2 were found to be unchanged in mutants compared to controls (Figures S2A–S2H). Furthermore, we did not detect differences in the numbers of cleaved Caspase3-positive cells in the neocortex of mutant and control brains from E14.5 to P2 (Figures S2I–S2K). This excludes changes in neurogenesis and/or survival to contribute to the observed phenotype in the *Bcl11a* mutant neocortex.

The onset of Bcl11a expression was detected within the IZ (Figures 1A–1D), where cortical neurons undergo polarity changes required for initiation of radial migration (Cooper, 2014). This prompted us to analyze the migration process of upper-layer cortical neurons in greater detail. We used in utero electroporation (IUE) to directly examine whether Bcl11a is cell-intrinsically required for migration of prospective late-born (i.e., E14.5–E15.5), upper-layer neurons. A vector containing Cre, followed by a cytoplasmically expressed IRES-GFP cassette, was introduced into the lateral VZ of *Bcl11a*$^{flox/flox}$ and *Bcl11a*$^{flox/+}$ embryos at E14.5, resulting in the efficient and specific deletion of Bcl11a in electroporated cells (Figures S3A and S3B). Electroporated brains were analyzed on consecutive time points from E16.5, after electroporated neurons left the progenitor zone entering the SVZ/IZ, to P2, when most of the cells reached their target sites (Figures 2A–2D). At E16.5, no difference in the distribution of GFP-expressing cells was detected (Figures 2A and 2E). However, at E17.5, significantly fewer GFP-positive *Bcl11a* mutant cells were located in the CP, and more cells were found in the IZ, as well as in the VZ/SVZ compared to controls (Figures 2B and 2F). A similar shift in distribution was still detectable at E18.5 (Figures 2C and 2G), while at P2 the relative number of GFP-positive cells found in mutants was normalized. At this stage, we also noted that mutant cells were packed more densely in bin 1 (corresponding to layers 2–3) as compared to controls (Figures 2D and 2H). At E17.5, a very similar misdistribution of GFP-labeled cells was observed in *Bcl11a*|*Emx1*^{Cre}, as well as in *Bcl11a*|*Nex*^{Cre} mutant brains (Figures 2I–2L), electroporated with a Cre-dependent reporter construct (loxP-GFP). The phenotype was completely rescued by the re-introduction of *Bcl11a* cDNA (*XL-isoform*) (Satterwhite et al., 2001) into mutant neurons (Figures S4A and S4B), indicating a cell-intrinsic effect.

To further corroborate our observations, we used independent experimental strategies and labeled migrating neurons born at E15.5 by BrdU injection into *Bcl11a*|*Emx1*^{Cre} mutants, as well as into *Bcl11a*|*Nex*^{Cre} mutants. Analyzing brains at P2 revealed similar changes in the distribution of *Bcl11a* mutant cells as observed in E18.5 brains that were electroporated at E14.5 (Figures S4C and S4D; cf. Figure 2C).

Bcl11a Controls Bipolar Morphology of Migrating Neurons

We observed that, within the IZ, young cortical neurons displayed altered morphology upon loss of *Bcl11a*. Electroporation of Cre-IRES-GFP into *Bcl11a*$^{flox/flox}$ brains significantly increased the proportion of neurons with multipolar morphology (i.e., with at least three processes) at the expense of bipolar cells specifically within the lower and middle regions of the IZ compared to controls (Figures 3A–3C). A similar phenotype was observed in *Bcl11a*|*Emx1*^{Cre} mutants, as well as in *Bcl11a*|*Nex*^{Cre} mutants (Figures S5A and S5B). Co-electroporation of Cre-IRES-GFP, together with a vector containing *Bcl11a-XL* cDNA, was sufficient to completely normalize the ratio of multi- to bipolar morphologies (Figures 3A–3C). To further characterize polarization in *Bcl11a* mutant cortical neurons, we labeled the Golgi apparatus with GFP-tagged galactosyltransferase (Jossin and Cooper, 2011; Yanagida et al., 2012) and quantified the proportion of *Bcl11a* mutant and control cells with the Golgi apparatus facing the CP (Figure 3D). Loss of *Bcl11a* resulted in a significant decrease of cells with a radially oriented Golgi apparatus already at E16.5 (Figures 3D and 3E), supporting a role of Bcl11a in cortical neuron polarization.

To test whether changes in the organization of the radial glial scaffold contribute to the defective neuronal migration, we used nestin as a marker. Radial glial scaffold was unchanged in *Bcl11a*|*Emx1*^{Cre} mutants compared to controls (Figures S2L and S2M).

To directly visualize the migratory behavior of late-born cortical neurons, we carried out live-cell imaging studies using cultured slices from *Bcl11a*$^{flox/flox}$ brains electroporated with either Cre-IRES-GFP or a control vector (Figure 4; Movies S1, S2, and S3). Together, these experiments confirmed that *Bcl11a* mutant cortical neurons fail to efficiently switch from multi- to bipolar morphology and to properly continue radially oriented migration (Figure 4A; Movies S1, S2, and S3). This results in significantly reduced overall migration speed and a characteristic shift in the speed profiles, as well as in the radial orientation of mutant neurons as compared to controls (Figures 4B–4E). Interestingly, analysis of individual migration profiles revealed that *Bcl11a* mutant neurons frequently undergo repetitive phases of several hours duration with dramatically reduced speed and random-like orientation changes (Figure 4B; Movie S3).

Sema3c Acts Downstream of Bcl11a to Control Bipolar Morphology and Radial Migration

To identify candidate molecules acting downstream of Bcl11a, we performed microarray-based gene expression profiling at E14.5 using cortical tissue from *Bcl11a* mutant and control littermates. Based on this analysis, *Sema3c* was consistently found deregulated in *Bcl11a* mutants (Table S1). Verification by quantitative real-time PCR revealed a 2.8-fold upregulation of *Sema3c* at E14.5 and E16.5 (Figure 5A). In situ hybridization showed changes in the expression pattern of *Sema3c*, which was increased in the SVZ/IZ of the *Bcl11a*|*Emx1*^{Cre} neocortex at both stages (Figure 5B).

Using the Ensembl Genome Browser (Flicek et al., 2013), we identified a putative regulatory region of 1.1 kb in the second intron that was located 35 kb downstream of the transcriptional start site of *Sema3c* and contained six GGCCGG motifs that are known binding sites of Bcl11a (Avram et al., 2002) and are separated from each other by 212 bp. The motifs were located in six larger DNA repeats with a high degree of conservation. Binding of Bcl11a to these repeats was tested by chromatin immunoprecipitation (ChIP), followed by quantitative real-time PCR using a primer pair that specifically detected binding to all six motifs. An enrichment of precipitated DNA of more than 4-fold was found using a Bcl11a-specific antibody in comparison to an immunoglobulin G (IgG) control antibody (Figure 5C), demonstrating binding of Bcl11a to this region. As a negative control, binding of Bcl11a to the *Hprt* promoter was tested, but no significant enrichment was found in comparison to the IgG control antibody (Figure 5C). This 1.1-kb regulatory sequence was tested for transcriptional activity by luciferase assays, and a repression of 31% was measured, indicating this element to convey functional

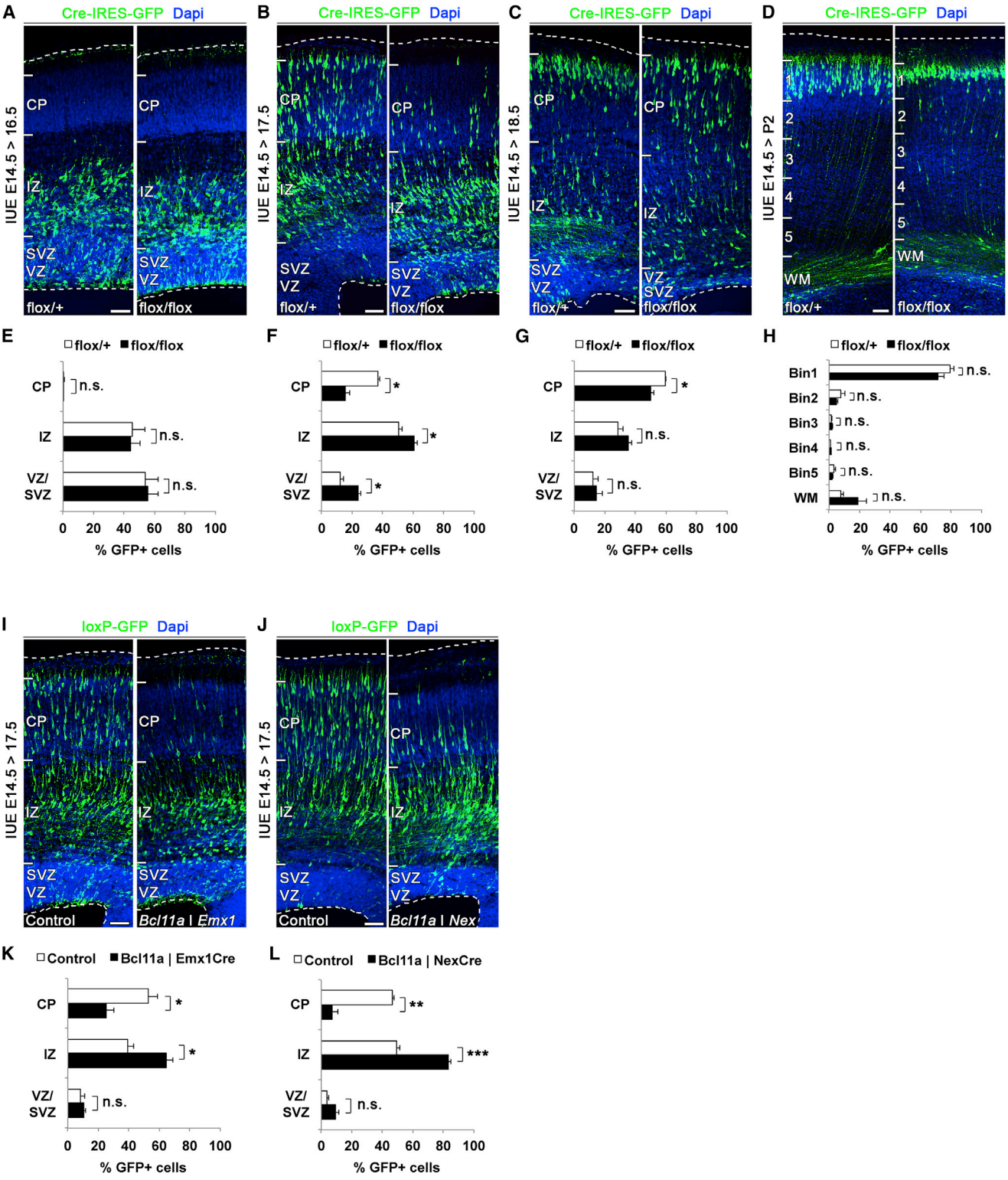

Figure 2. Upper-Layer Cortical Neurons Require Bcl11a for Migration

(A–D) *Bcl11a*$^{flox/+}$ and *Bcl11a*$^{flox/flox}$ brains were electroporated at E14.5 with Cre-IRES-GFP and analyzed at (A) E16.5, (B) E17.5, (C) E18.5, and (D) P2. Fewer GFP-positive *Bcl11a* mutant cells are located in the cortical plate (CP), while more positive cells are found the intermediate zone (IZ) and ventricular/subventricular zones (VZ/SVZ) compared to controls at E17.5.

(E–H) Quantification of the relative distribution of GFP-positive cells in VZ/SVZ, IZ, and CP as indicated in (A)–(C) or five bins as indicated in (D) (n = 3).

(legend continued on next page)

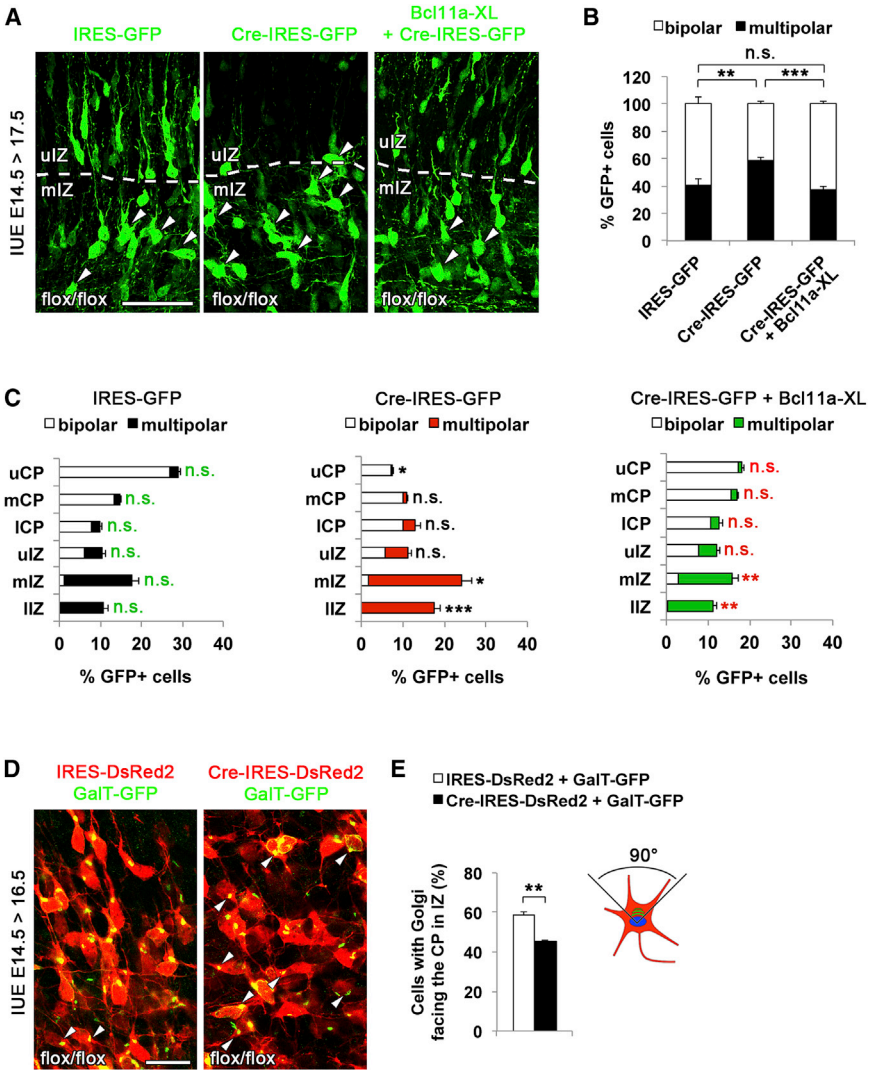

Figure 3. Polarization of Upper-Layer Cortical Neurons Depends on Bcl11a

(A) Electroporation of Cre-IRES-GFP into *Bcl11a*$^{flox/flox}$ brains at E14.5 increases the proportion of multipolar at the expense of bipolar GFP-positive cells in the E17.5 cortex compared to a control vector. Co-electroporation of Cre-IRES-GFP, together with Bcl11a-XL, is sufficient to rescue the phenotype.

(B) Quantification of experiments shown in (A) (n = 3). Mean ± SEM; one-way ANOVA, followed by an LSD post hoc test; ns, not significant; **p < 0.01; ***p < 0.001.

(C) Graphs represent the distribution of bipolar and multipolar cells quantified in (B) in the lower, middle, and upper sections of the intermediate zone (lIZ, mIZ, and uIZ) and cortical plate (lCP, mCP, and uCP), respectively (n = 3). Mean ± SEM; one-way ANOVA, followed by an LSD post hoc test; ns, not significant; *p < 0.05; **p < 0.01; ***p < 0.001.

(D) Co-electroporation of Cre-IRES-DsRed2 and GalT-GFP into *Bcl11a*$^{flox/flox}$ brains at E14.5 decreases the proportion of DsRed2-positive cells in the IZ with a Golgi apparatus facing the cortical plate (CP) at E16.5 compared to a control vector.

(E) Quantification of the experiment shown in (D) (n = 3). Mean ± SEM; Student's t test; **p < 0.01.

Scale bars, 50 μm (A) and 20 μm (D). See also Figure S5.

repression through Bcl11a binding (Figure 5D). Consistent with the biochemical analysis, *Sema3c* gene expression and Bcl11a protein expression overlap in the IZ of the neocortex (Figure 5E). Moreover, the Sema3c receptors Nrp1 and Plxna2 are as well expressed in the IZ (Chen et al., 2008; Hatanaka et al., 2009).

Electroporation of a vector containing *Sema3c* cDNA, followed by an IRES-GFP cassette into the VZ of E14.5 wild-type embryos, resulted in migration defects of cortical neurons similar to those observed upon loss of *Bcl11a* (Figures 5F and 5G). In addition, the proportion of multipolar cells was significantly increased upon overexpression of *Sema3c* in comparison to control vector (Figure 5H). Finally, using GFP-tagged galactosyltransferase demonstrated a similar decrease in the proportion of cells with the Golgi apparatus facing the CP in both neurons with gain of function of *Sema3c* and with loss of *Bcl11a* (Figures 5I and 5J; cf. Figures 3D and 3E).

Next, we performed genetic rescue experiments by introducing two independent *Sema3c* short hairpin RNA (shRNA) constructs into *Bcl11a*-deficient cells. Compared to a control shRNA, both constructs knocked down *Sema3c* expression but to various extents (shRNA#2 > shRNA#1) in HEK293 cells (Figure 6D, left). Each construct was co-electroporated with Cre-IRES-GFP into the VZ of *Bcl11a*$^{flox/flox}$ embryos at E14.5. Remarkably, knockdown of *Sema3c* by shRNA#2 completely rescued neuronal migration and morphological defects in *Bcl11a* mutant neurons, while we still observed partial rescue of the phenotype with the less-efficient shRNA#1 (Figures 6A–6C). As a further control, we electroporated shRNA#1 or #2, together with a knockdown-resistant *Sema3c** cDNA (Figure 6D, right) into *Bcl11a* mutant neurons. By this, we were not able to rescue the *Bcl11a* mutant phenotype (Figures 6A–6C). Altogether, our data provide evidence that *Sema3c* is an important downstream effector of Bcl11a, regulating polarization and radial migration of cortical neurons.

(I and J) Similar misdistributions are found in E17.5 (I) *Bcl11a*|*Emx1*^{Cre} or (J) *Bcl11a*|*Nex*^{Cre} mutant brains electroporated at E14.5 with loxP-GFP.
(K and L) Quantification of experiments shown in (I) and (J), respectively (n = 3). Nuclei are stained with DAPI. WM, white matter.
All graphs represent the mean ± SEM; Student's t test; ns, not significant; *p < 0.05; **p < 0.01; ***p < 0.001. Scale bars, 50 μm.
See also Figures S3 and S4.

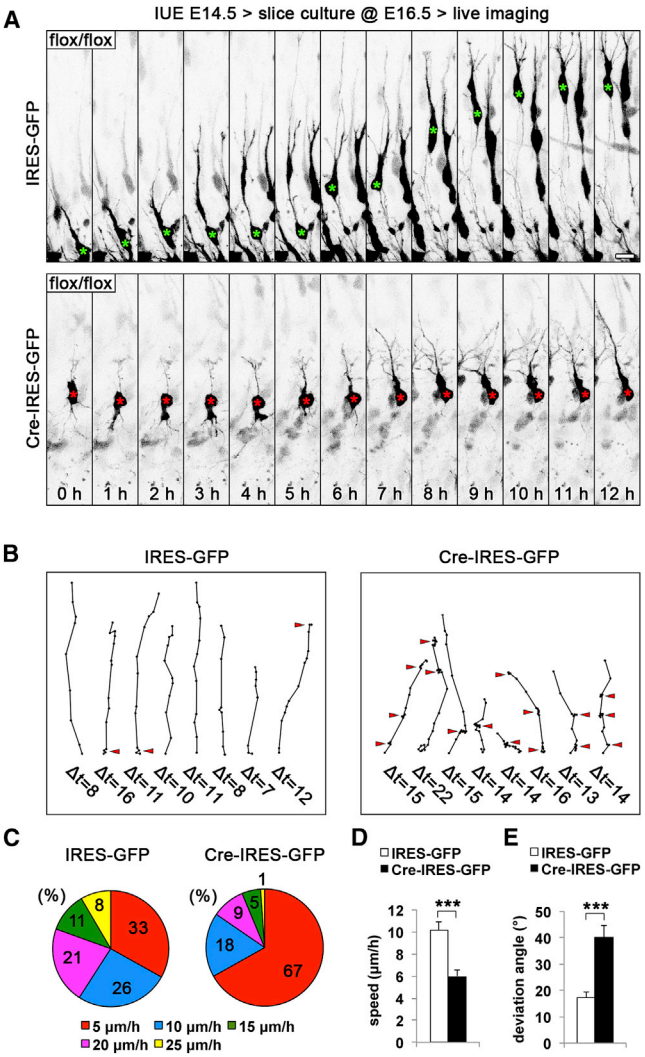

Figure 4. Migration Behavior of *Bcl11a* Mutant Upper-Layer Cortical Neurons

(A) Representative images of migrating GFP-positive neurons in E16.5 slice cultures from *Bcl11a*$^{flox/flox}$ brains electroporated at E14.5 with either Cre-IRES-GFP or a control vector over a total imaging period of 12 hr.

(B) Representative traces with 1 hr interval resolution of migrating GFP-positive neurons in E16.5 slice cultures from *Bcl11a*$^{flox/flox}$ brains electroporated at E14.5 with Cre-IRES-GFP or a control vector over total imaging periods of up to 22 hr. *Bcl11a* mutant neurons frequently undergo repetitive phases of reduced migration speed and randomly change orientation (marked by red arrowheads).

(C) Speed profiles calculated from traces of migrating neurons as shown in (B).

(D and E) Quantification of speed (D) and deviation angle from radial orientation (E) of migrating GFP-positive neurons in E16.5 slice cultures from *Bcl11a*$^{flox/flox}$ brains electroporated at E14.5 with Cre-IRES-GFP or a control vector (n = 15). Mean ± SEM; Student's t test; ***$p < 0.001$.

Scale bar, 10 µm. See also Movies S1, S2, and S3.

Morphogenesis and Survival of Postmigratory Upper Layer Neurons Depend on Bcl11a

Impaired migration of *Bcl11a* mutant cortical neurons resulted in delayed arrival and higher compaction of neurons within the CP (Figure 2D), raising the possibility that morphogenesis of postmigratory upper layer neurons might also depend on Bcl11a. To directly visualize the morphology of single neurons within the upper cortical layers, we co-electroporated *Bcl11a*|*Emx1*^{Cre} brains at E14.5 with a FLPe expression construct at low concentration, together with a FLPe-dependent GFP reporter (Matsuda and Cepko, 2007). Compared to controls at P2, late-born *Bcl11a* mutant neurons displayed severe changes in their morphology as characterized by dramatically shortened primary apical dendrites and increased dendritic branching close to the soma (Figures 7A–7C). Next, we asked whether impaired morphology of mutant upper-layer neurons is due to an isolated, postmigratory function of Bcl11a or whether morphogenesis requires early expression of this factor. Using a tamoxifen-dependent ERT2-Cre-ERT2 construct (Matsuda and Cepko, 2007), we selectively induced the mutation of *Bcl11a* after E18.5 when the majority of neurons had reached the superficial CP (Figure S6) and found that the morphology of the *Bcl11a* mutant upper-layer cortical neurons was unchanged (Figures 7D–7F). To explore, whether impaired morphogenesis of neurons with an early mutation of *Bcl11a* is part of a specification defect, we analyzed molecular markers expressed by late-born upper-layer neurons. At P2, the proportion of late-born neurons, as identified by BrdU injection at E15.5, that co-expressed Cux1, Brn2, or Satb2 was unchanged in *Bcl11a*|*Emx1*^{Cre} mutants compared to controls (Figures S7A–S7C and S7F), suggesting that late-born *Bcl11a* mutant neurons retain their capacity to undergo normal upper-layer specification as defined by these markers.

To analyze whether these neurons are subsequently depleted by apoptosis, we quantified cleaved Caspase3 expression in *Bcl11a*|*Emx1*^{Cre} mutant brains and found a massive increase of apoptosis in superficial cortical layers from P4 to P6 (Figures 7G–7H). In addition, we noticed a discrete elevation of cell death in deep cortical positions between P4 and P5. Electroporation of *Bcl11a*$^{flox/flox}$ brains with Cre-IRES-GFP at E14.5 increased the apoptosis rate selectively in late-born GFP-positive *Bcl11a* mutant cells at P5 (Figures 7I and 7J). Compared to controls, apoptosis rates remained unchanged at P5, when the *Bcl11a* mutation was selectively induced by tamoxifen after E18.5 (Figures 7K and 7L). At P8, the number of Cux1- and Brn2-expressing neurons within the upper layers was dramatically reduced, and the thickness of the corpus callosum, which harbors axonal projections predominantly derived from upper-layer neurons, was significantly narrowed in *Bcl11a*|*Emx1*^{Cre} mutants (Figures S7H–S7K). Collectively, our data suggest that late differentiation, as characterized by altered morphology, and the subsequent survival of postmigratory upper-layer neurons, depend on the early expression of Bcl11a and may thus be the consequence of impaired migration and delayed arrival of neurons.

Interestingly, morphology and survival of upper-layer cortical neurons were unchanged at P2 and P5, respectively, in wild-type brains electroporated with Sema3c-IRES-GFP at E14.5 (data not shown). Thus, the late phenotype of *Bcl11a* mutant upper-layer neurons appears to be independent of *Sema3c*.

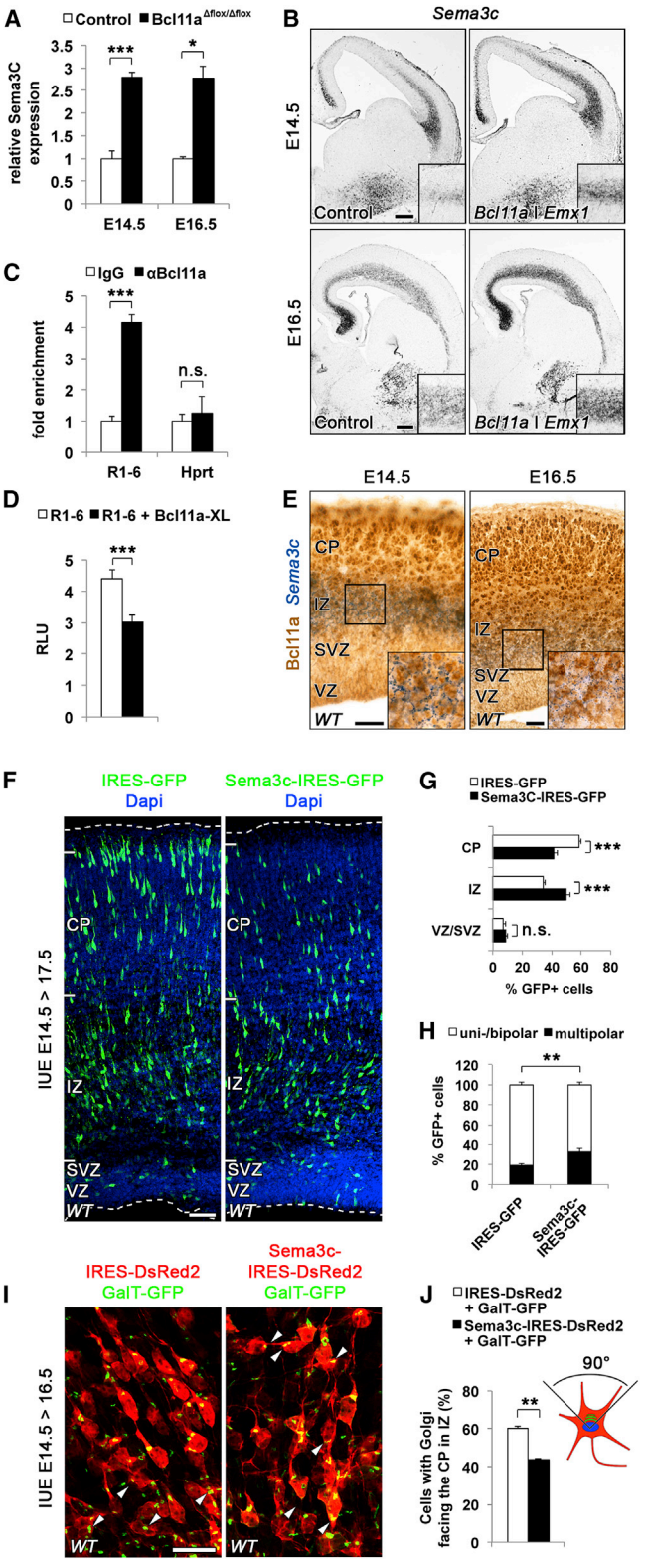

Figure 5. *Sema3c* Is a Functional Target Gene of Bcl11a

(A) Relative *Sema3c* mRNA levels determined by quantitative real-time PCR in cortical tissue of *Bcl11a*$^{\Delta flox/\Delta flox}$ mutants are increased at E14.5 (n = 4) and E16.5 (n = 3) in comparison to wild-type controls.

(B) In situ hybridization of *Sema3c* showing upregulation in *Bcl11a*|*Emx1*^{Cre} mutants at E14.5 and E16.5 compared to controls.

(C) ChIP analysis using a Bcl11a antibody and E14.5 cortical tissue detects Bcl11a binding to a 1.1 kb region (R1–R6) within the second intron of *Sema3c* (n = 3). Negative controls include ChIP with unspecific IgG antibody and the precipitation of the *Hprt* promoter.

(D) Luciferase assays in HEK293 cells transfected with *Bcl11a-XL* or a control vector show repression of luciferase activity of the R1–R6 reporter construct by Bcl11a-XL (n = 3) 2 days after transfection.

(E) In situ hybridization combined with immunohistochemistry showing overlapping expression of Bcl11a protein and *Sema3c* mRNA in the intermediate zone (IZ) in wild-type (WT) brains at E14.5 and E16.5. Insets are enlargements of the boxed areas in corresponding panels.

(F) Electroporation of Sema3c-IRES-GFP into WT brains at E14.5 increases the proportion of GFP-positive cells in the IZ at the expense of GFP-positive cells in the cortical plate (CP) compared to a control vector at E17.5. Nuclei are stained with DAPI.

(G) Quantification of the experiment shown in (F) (n = 3).

(H) Graph represents the proportion of bipolar and multipolar GFP-positive cells in the E17.5 cortex of WT brains electroporated with Sema3c-IRES-GFP or control vector at E14.5 (n = 3). Electroporation of Sema3c-IRES-GFP increases the proportion of multipolar at the expense of bipolar cells compared to a control vector.

(I) Co-electroporation of Sema3c-IRES-DsRed2 and GalT-GFP into WT brains at E14.5 decreases the proportion of DsRed2-positive cells with a Golgi apparatus facing the CP in the IZ at E16.5 compared to control vector.

(J) Quantification of the experiment shown in (I) (n = 3).

VZ/SVZ, ventricular/subventricular zones. All graphs represent the mean ± SEM; Student's t test; ns, not significant; *p < 0.05; **p < 0.01; ***p < 0.001. Scale bars, 200 μm (B), 40 μm (E), 50 μm (F), and 20 μm (I).

A Function of Bcl11a in Deep-Layer Neuron Specification

We noticed that BrdU injection at E15.5 labeled small amounts of cells in control brains still expressing Tbr1 and Bcl11b, which label deep-layer neurons predominantly born at earlier stages (Molyneaux et al., 2007). In *Bcl11a*|*Emx1*^{Cre} mutants a small increase in the proportion of Bcl11b-positive cells, but no change in Tbr1 expression, was detected (Figures S7D, S7E, and S7G), raising the possibility that Bcl11a exerts additional functions in the specification of a part of deep-layer neurons. Indeed, when we tagged early-born deep-layer neurons by BrdU-injection at E12.5, we found an increase in the proportion of Bcl11b co-expressing cells at the expense of those neurons co-expressing Tbr1 or Fog2 (Figures 8A–8C and 8F), without any changes in their positioning within the cortex. A similar shift in specification toward the Bcl11b-positive cell population was observed in *Bcl11a*$^{flox/flox}$ brains electroporated with Cre-IRES-GFP at E12.5 (Figures 8D, 8E, and 8G). To further characterize this deep-layer phenotype, we carried out antero- and retrograde DiI-labeling experiments to visualize major projections of deep-layer neurons. The corticospinal and corticothalamic tracts appeared grossly normal in *Bcl11a*|*Emx1*^{Cre} mutants, and retrograde-labeled neurons from the cerebral peduncle and thalamus expressed Bcl11b and Tbr1, respectively (Figures S8A and S8B). In addition, we analyzed 10-week-old *Bcl11a*|*Emx1*^{Cre} mutants crossed to *Thy1-YFP* transgenic mice expressing YFP, specifically in layer 5 (i.e., Bcl11b-positive) neurons, and the corresponding corticospinal tract (Feng et al., 2000). Surprisingly, none of these experiments revealed major alterations in deep-layer neuron projections (Figures S8C and S8D).

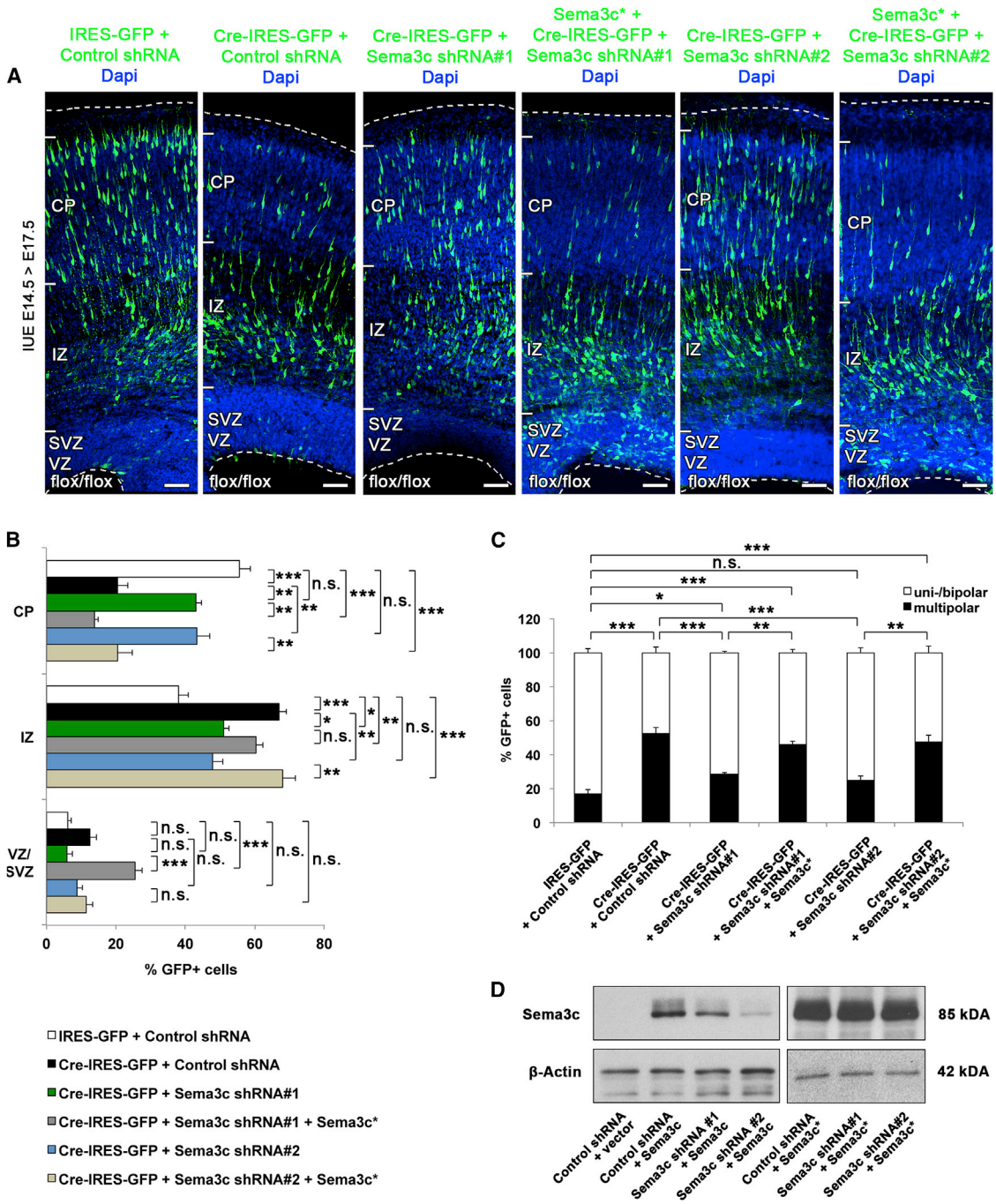

Figure 6. Knockdown of Sema3c in *Bcl11a* Mutant Upper-Layer Cortical Neurons Rescues Polarization and Migration Defects

(A) Co-electroporation of Cre-IRES-GFP and a control shRNA into *Bcl11a*$^{flox/flox}$ brains at E14.5 increases the proportion of GFP-positive cells in the intermediate zone (IZ) at the expense of GFP-positive cells in the cortical plate (CP) at E17.5 compared to a control vector, together with a control shRNA. Co-electroporation of Cre-IRES-GFP and a Sema3c-specific shRNA (two independent constructs: shRNA#1 and shRNA#2) rescues the phenotype. Co-electroporation of Cre-IRES-GFP, Sema3c shRNA#1 or #2, and a knockdown-resistant Sema3c expression construct (Sema3c*) does not rescue the phenotype. Nuclei are stained with DAPI. VZ/SVZ, ventricular/subventricular zones.

(B) Quantification of experiments shown in (A) (n = 3 for each group).

(C) Graph represents the proportion of bipolar and multipolar GFP-positive cells in the E17.5 cortex of *Bcl11a*$^{flox/flox}$ brains electroporated as indicated at E14.5 (n = 3 for each group). Co-electroporation of Cre-IRES-GFP, together with a control shRNA, increases the proportion of multipolar at the expense of bipolar cells compared to a control vector, together with a control shRNA. Co-electroporation of Cre-IRES-GFP and Sema3c shRNA#1 or #2 rescues the phenotype.

(legend continued on next page)

DISCUSSION

In this study we provide direct genetic evidence that the transcription factor *Bcl11a* is required for cell-polarity switch and radial migration of upper-layer projection neurons. We show that Bcl11a acts through direct transcriptional regulation of *Sema3c* in this process. *Sema3c* is expressed by migrating neurons in the IZ of the neocortex. Overexpression of *Sema3c* in wild-type cortical neurons recapitulates the *Bcl11a* mutant phenotype, whereas knockdown of *Sema3c* in *Bcl11a*-deficient cortical neurons rescues it. Moreover, early expression of Bcl11a is required for late differentiation and survival of upper-layer cortical neurons independent of Sema3c.

Migrating upper-layer neurons become transiently multipolar in the SVZ and lower IZ and move randomly for a limited period of time. Subsequently, they extend axons, orient themselves toward the pia, and become bipolar in the upper IZ (LoTurco and Bai, 2006; Namba et al., 2014; Noctor et al., 2004; Tabata and Nakajima, 2003). This polarity switch is an important step during radial migration that has been implicated in specification of neuron subtype identity, cortical lamination, and projection formation (Evsyukova et al., 2013; Miyoshi and Fishell, 2012; Noctor et al., 2004; Ohshima et al., 2007; Pacary et al., 2011). Loss of function of *Bcl11a* in late-born migrating upper-layer neurons increased the proportion of neurons with retained multipolar morphology at the expense of bipolar cells, specifically in the lower and middle IZ. Impaired polarization precedes misdistribution of mutant migrating neurons. This suggests that *Bcl11a*-deficient neurons fail to switch to a bipolar morphology and to properly continue radial migration. Using live-cell imaging analyses, we directly demonstrate that appropriate polarization and radial migration depend on Bcl11a.

Bcl11a mutant neurons repetitively slowed migration and randomly changed their orientation for a prolonged time, suggesting that these cells unsuccessfully probe the environment for signals regulating their migration. Compatible with this, we identified an extracellular guidance molecule, *Sema3c*, as a critical component required for radial migration. *Sema3c* and Bcl11a co-localize in neurons within the IZ, and Bcl11a directly binds to a regulatory element in the second intron of the *Sema3c* gene that conveys transcriptional repression. In *Bcl11a|Emx1*^{Cre} mutants, *Sema3c* was upregulated in the SVZ/IZ, and the fraction of multipolar cells was increased upon loss of function of *Bcl11a* or gain of function of *Sema3c.* Moreover, knockdown of *Sema3c* in *Bcl11a* mutant neurons was sufficient to completely rescue impaired polarization and migration, indicating that *Sema3c* regulates radial migration downstream of Bcl11a. This does, however, not exclude additional downstream targets of Bcl11a from being involved in this process.

Another class III semaphorin, Sema3a, functions as a polarizing factor in cortical neurons by suppressing axon formation and promoting dendrite growth (Shelly et al., 2011). In addition, Sema3a orients apical dendrites of cortical neurons toward the pial surface and guides their migration (Chen et al., 2008; Polleux et al., 2000). In contrast, Sema3c has been shown to act as an attracting factor for neocortical axons, both in vitro and in vivo (Bagnard et al., 1998, 2000; Niquille et al., 2009; Piper et al., 2009). Because all class III semaphorins bind to Nrp1/2 receptors (Pasterkamp, 2012), which are expressed in migrating neocortical neurons (Chen et al., 2008; Hatanaka et al., 2009), increased levels of *Sema3c* in *Bcl11a* mutants might oppose the Sema3a signal that guides migrating neurons toward the pial surface. Thus, our analysis suggests a mechanistic concept, by which combinatorial codes of different semaphorins may exist in the wild-type neocortex controlling morphology and migration of projection neurons.

Previous studies suggest that neuronal migration and laminar identity are co-regulated by the same transcriptional programs in developing cortical projection neurons (Evsyukova et al., 2013; Kwan et al., 2012). In *Satb2* mutants, for example, upper-layer neurons show a defect in migration that is corrected within the first postnatal week. Upper-layer neurons ectopically activate Bcl11b expression (which is normally restricted to L5) and adapt to their abnormal environment by projecting aberrantly into the corticospinal tract (Alcamo et al., 2008; Britanova et al., 2008). Although, *Bcl11a*-deficient late-born neurons retained their endogenous marker profile (Satb2, Cux1, and Brn2), we observed striking alterations in neuron morphology after delayed arrival at their target sites. Subsequently, a part of the mutant neurons is eliminated by apoptosis. This ultimately results in hypoplasia of the upper cortical layers and of the callosal tract. Interestingly, postnatal morphogenesis and survival of upper-layer neurons requires the early expression of Bcl11a. However, these processes do not depend on Sema3c signals. Thus, Bcl11a appears to regulate distinct steps during the development of late-born upper-layer neurons through separate downstream pathways. Several scenarios may explain why *Bcl11a* mutant neurons die postnatally. Altered morphology may prevent mutant neurons from synaptic integration into the cortical circuitry; as a consequence, non-functional neurons are depleted by apoptosis (Verhage et al., 2000). Moreover, delayed arriving Bcl11a mutant upper-layer neurons may miss spatiotemporally limited signals, provided by the target zone, that are required for further maturation, as well as for proper functional integration. Alternatively, Bcl11a might control the expression of signals that provide trophic support to upper-layer neurons. In line with this, Bcl11a has been shown in other tissues to directly regulate apoptosis pathways, including members of the anti-apoptotic *Bcl2* family (Yu et al., 2012). Interestingly, the mutation of *Bcl-xL* in mice results in massive cell death of cortical neurons (Motoyama et al., 1995; Zaidi et al., 2001). Moreover, Rho GTPases have been shown to control cytoskeletal dynamics (Luo, 2000), as well as survival of cortical neurons (Sanno et al., 2010). Thus, Bcl11a-dependent signals regulating morphology and survival of cortical neurons may exist that converge at the level of the cytoskeleton.

(D) Western blot analysis of HEK293 cells co-transfected as indicated and probed using anti-Sema3c and anti-β-Actin antibodies. Sema3c shRNA#1 and #2 reduce Sema3c expression to a different extent (shRNA#1 < shRNA#2) 2 days after transfection. Sema3c* is not reduced by Sema3c shRNA#1 or #2.

All graphs represent the mean ± SEM; one-way ANOVA, followed by an LSD post hoc test; ns, not significant; *p < 0.05; **p < 0.01; ***p < 0.001. Scale bars, 50 μm.

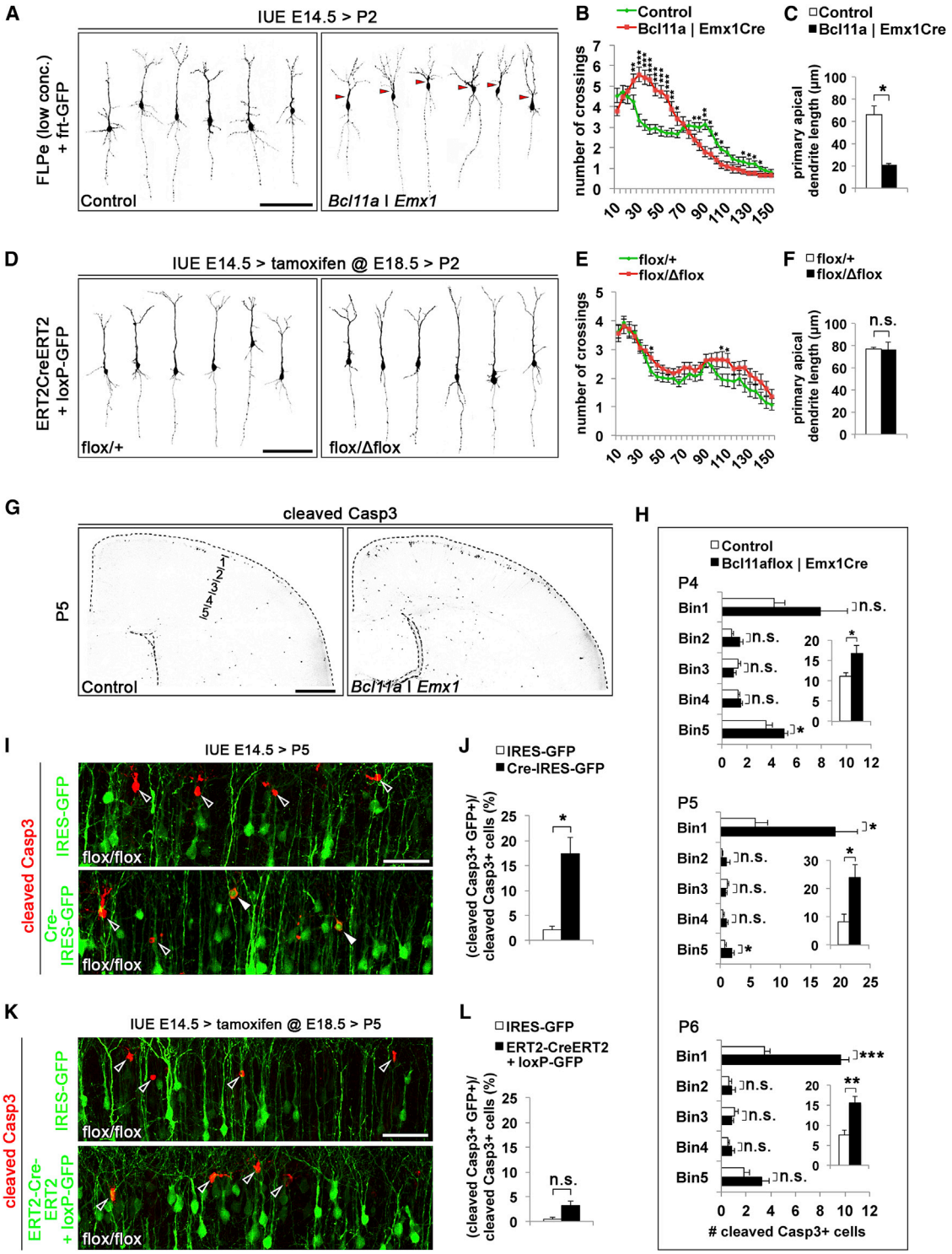

Figure 7. Morphogenesis and Postnatal Survival of Upper Layer Cortical Neurons Depends on Bcl11a

(A) Representative images of P2 *Bcl11a*|*Emx1*^{Cre} mutant and control neurons co-electroporated at E14.5 with FLPe at low concentration and frt-GFP. GFP-positive *Bcl11a* mutant neurons display a shortened primary apical dendrite (marked by red arrowheads) and increased dendritic branching close to the soma.

(B) Sholl analysis of GFP-positive neurons from the experiment shown in (A) (n = 30).

(C) Quantification of the primary apical dendrite length of GFP-positive neurons in treated brains from the experiment shown in (A) (n = 3).

(legend continued on next page)

Our analysis of the function of *Bcl11a* in neocortical development uncovered an additional independent role of this factor in deep-layer neuron specification, resulting in a loss of Tbr1- and Fog2-positive layer 6 neurons and a simultaneous increase in Bcl11b-positive layer 5 neurons. The increased number of Bcl11b-positive neurons might be caused by compensatory upregulation of this closely related gene. Upregulation of Bcl11b could be responsible for Tbr1 repression in the deep cortical layers of the *Bcl11a* mutants; such a mechanism was previously observed in *Satb2* mutants that show upregulation of Bcl11b as well (Srinivasan et al., 2012). At P2, we did not detect changes in the distribution of deep-layer neurons within the CP. This does, however, not exclude transient defects in migration of this neuron population. Moreover, we observed a mild increase in apoptosis within the deep cortical layers at P4–P5. This raises the possibility that Bcl11a might have a uniform function in both deep- upper-layer cortical neurons. Experimental evidence provided in this study argues against such a model: loss of Bcl11a results in (1) altered specification of deep- but not of upper- layer neurons and (2) substantial and lasting defects of major projections of upper-layer (reduced size of corpus callosum), but not of deep-layer, neurons (unchanged corticospinal and corticothalamic tracts).

Recently, a genome-wide association study (GWAS) and whole-exome sequencing have identified *Bcl11a* as a candidate gene involved in developmental disorders, including autism spectrum disorders associated with impaired neocortical development (De Rubeis et al., 2014; Deciphering Developmental Disorders, 2015; Hussman et al., 2011; Iossifov et al., 2012). Moreover, *Bcl11a* is a candidate for the 2p15-16.1 microdeletion syndrome, which is associated with mental retardation and neocortical dysplasia (Hancarova et al., 2013; Peter et al., 2014; Rajcan-Separovic et al., 2007). Our study provides direct genetic evidence for *Bcl11a* as an essential regulator in the development of the neocortex in mice and thus further establishes an important role for this gene in the pathophysiology of neurodevelopmental disorders in humans.

EXPERIMENTAL PROCEDURES

Mouse Mutants, BrdU, and Tamoxifen Injection

All mouse experiments were carried out in compliance with German law and approved by the respective government offices in Tübingen. Mice carrying a conditional knockout allele of *Bcl11a* (*Bcl11a*^{flox}) have previously been described (John et al., 2012). These mice were crossed to *Deleter*^{Cre}, *Emx1*^{IRESCre}, or *Nex*^{Cre} mice (Goebbels et al., 2006; Gorski et al., 2002; Schwenk et al., 1995) to generate *Bcl11a*$^{\Delta flox/\Delta flox}$ mutants, conditional *Bcl11a*$^{flox/flox}$; *Emx1*$^{IRESCre/+}$ (*Bcl11a*|*Emx1*^{Cre}), or conditional *Bcl11a*$^{flox/flox}$; *Nex*$^{Cre/+}$ (*Bcl11a*|*Nex*^{Cre}) mutants, respectively. Wild-type, *Bcl11a*$^{flox/+}$; *Emx1*$^{IRESCre/+}$, or *Bcl11a*$^{flox/+}$; *Nex*$^{Cre/+}$ littermates served as controls. Genotyping of the mice was performed by PCR. For BrdU birth dating experiments, BrdU (50 mg/kg of body weight) was intraperitoneally injected at E12.5, E14.5, E15.5, and E16.5, and embryos were dissected after 1 hr (for proliferation experiments) or at P2 (for pulse-chase and fate experiments). Tamoxifen (100 mg/kg of body weight) was injected intraperitoneally at E18.5.

Histology, Immunohistochemistry, and In Situ Hybridization

Histology, immunohistochemistry, and in situ hybridization were performed as previously described (John et al., 2012; Simon et al., 2012). Additional information is in the Supplemental Experimental Procedures.

Plasmids

Plasmids used in this study are listed in the Supplemental Experimental Procedures.

In Utero Electroporation

In utero electroporation was performed as previously described (Saito and Nakatsuji, 2001). Additional information is in the Supplemental Experimental Procedures.

Slice Culture and Live Imaging

Slice culture was performed as previously described (Polleux and Ghosh, 2002). Movies were analyzed using the ImageJ (v1.48, RRID: nif-0000-30467) (NIH) software. Additional information is in the Supplemental Experimental Procedures.

Microarray Analysis

Microarray analysis was performed as previously described (John et al., 2012; Simon et al., 2012). A transcriptome analysis was performed using Biometric Research Branch ArrayTools (RRID: nif-0000-30199) developed by Dr. Richard Simon and BRB-ArrayTools Development Team (http://linus.nci.nih.gov/BRB-ArrayTools.html). The data obtained in our microarray experiment were deposited at GEO under the accession number GEO: GSE52827. Additional information is in the Supplemental Experimental Procedures.

Quantitative Real-Time PCR

Total RNA was prepared from cortical tissue of *Bcl11a*$^{\Delta flox/\Delta flox}$ mutant and wild-type littermate embryos at E14.5 and E16.5 using the RNeasy Mini Kit (QIAGEN). RNAs were reverse transcribed with Superscript II reverse transcriptase (Invitrogen), and quantitative real-time PCR was performed using the LightCycler DNA Master SYBR Green I Kit (Roche) in a LightCycler 480 System (Roche). The following oligonucleotides were used: *Sema3c*,

(D) Representative images of P2 *Bcl11a*$^{flox/\Delta flox}$ and *Bcl11a*$^{flox/+}$ neurons co-electroporated at E14.5 with ERT2-Cre-ERT2 and loxP-GFP and injected at E18.5 with tamoxifen.
(E) Sholl analysis of GFP-positive neurons from the experiment shown in (D) (n = 30).
(F) Quantification of the primary apical dendrite length of GFP-positive neurons in treated brains from the experiment shown in (D) (n = 3).
(G) The number of cleaved Casp3-positive cells in P5 cortex is notably increased in the upper cortical layers in *Bcl11a*|*Emx1*^{Cre} mutants compared to controls.
(H) Quantification of cleaved Casp3-positive cells in cortical layers 2–6 in five bins (as indicated in G) in the cortex of *Bcl11a*|*Emx1*^{Cre} mutants and controls at P4 (n = 6), P5 (n = 5), and P6 (n = 6). Small graphs represent the total numbers of cleaved Casp3-positive cells in layers 2–6.
(I) Electroporation of Cre-IRES-GFP into *Bcl11a*$^{flox/flox}$ brains at E14.5 increases the number of cleaved Casp3-positive cells co-expressing GFP at P5 compared to a control vector.
(J) Quantification of the experiment shown in (I) (n = 3).
(K) The proportion of cleaved Casp3-positive cells co-expressing GFP at P5 is unchanged upon electroporation of ERT2-Cre-ERT2, together with loxP-GFP into *Bcl11a*$^{flox/flox}$ brains at E14.5, followed by injection of tamoxifen at E18.5 compared to a control vector.
(L) Quantification of the experiment shown in (K) (n = 3).
All graphs represent the mean ± SEM; Student's t test; ns, not significant; *p < 0.05; **p < 0.01; ***p < 0.001. Scale bars, 100 μm (A and D), 500 μm (G), and 50 μm (I and K). See also Figure S7.

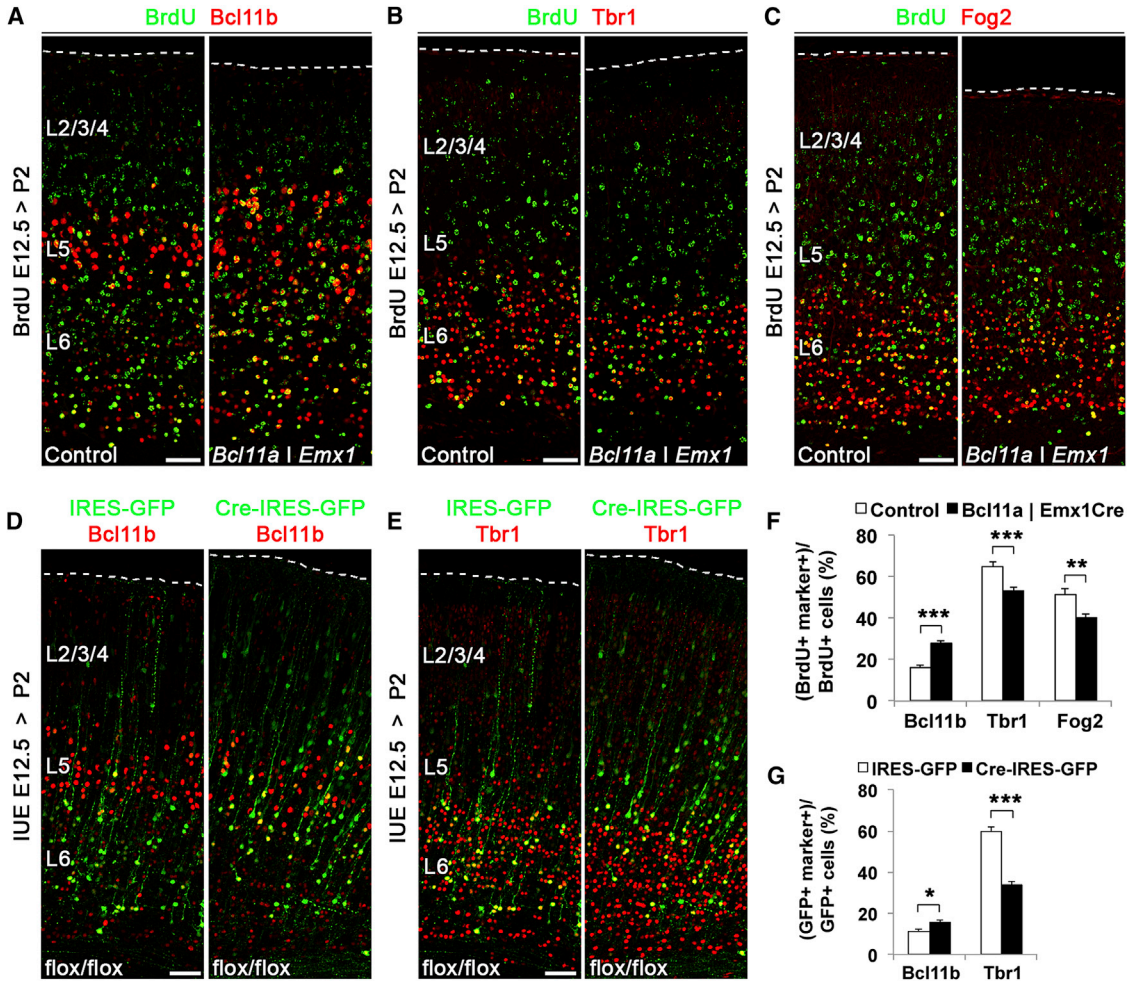

Figure 8. A Function of Bcl11a in Deep-Layer Neuron Specification

(A–C) BrdU injection at E12.5, followed by staining for BrdU and Bcl11b (A), Tbr1 (B), or Fog2 (C) in *Bcl11a*|*Emx1*^{Cre} mutant and control brains at P2. The proportion of BrdU-positive cells that co-express Bcl11b is increased, while the proportion of BrdU-positive cells that co-express Tbr1 or Fog2 is decreased in *Bcl11a*|*Emx1*^{Cre} mutants compared to controls. Cortical layers L2–L6 are indicated.

(D and E) Similar changes in the proportions of GFP-positive cells that co-express Bcl11b (D) and Tbr1 (E) are found in P2 *Bcl11a*$^{flox/flox}$ brains that were electroporated at E12.5 with Cre-IRES-GFP in comparison to a control vector.

(F) Quantification of experiments shown in (A)–(C) (n = 3).

(G) Quantification of experiments shown in (D) and (E) (n = 4).

All graphs represent the mean ± SEM; Student's t test; *p < 0.05; **p < 0.01; ***p < 0.001. Scale bars, 50 μm. See also Figure S8.

5′-GGGTTCAATCTGAAAGCATACA-3′ and 5′-TGTCTTTCTGCAGCAACCA C-3′ and *Gapdh*, 5′-TGGAGAAACCTGCCAAGTATG-3′ and 5′-GAGTTGCT GTTGAAGTCGCA-3′. The relative copy number of *Gapdh* RNA was quantified and used for normalization. Data were analyzed using the comparative C_T method (Schmittgen and Livak, 2008).

Chromatin Immunoprecipitation Assay

Chromatin immunoprecipitation (ChIP) assays were carried out as previously described (Simon et al., 2012). Briefly, ChIP assays were performed on cortical tissue collected from ten wild-type embryos at E14.5 employing a specific mouse monoclonal antibody recognizing Bcl11a (Abcam Cat# ab19489, RRID: AB_2063996) and using the EpiQuick Tissue Chromatin Immunoprecipitation Kit (Epigentek), including mouse IgG as a non-specific control. The precipitated DNA was analyzed by quantitative real-time PCR using oligonucleotides recognizing a 1.1-kb region in the second intron of *Sema3c*: 5′-GCGCCAGAGAACCTGACA-3′ and 5′-CTGCTGCTGTGGCTTAGG-3′. As a negative control, the *Hprt* promoter region was used, which was recognized by the following oligonucleotides: 5′-CTGCCTCTGCCTCCTAAATG-3′ and 5′-TGTCGTCTCCCAGAGGATTC-3′. ChIP quantitative real-time PCR data were analyzed by the comparative C_T method determining the fold enrichment of the immunoprecipitated DNA by the specific antibody versus IgG using the input DNA as reference. C_T values > 35 were disregarded. Every ChIP experiment was repeated at least three times.

Luciferase Assay

The 1.1-kb region in the second intron of *Sema3c* was cloned into the pMCS-*Gaussia* Luc Vector (pMCS-GLuc; ThermoScientific). This construct was transfected into HEK293 cells with and without pCMV-Myc-*Bcl11a-XL* using Lipofectamine 2000 in accordance with the manufacturer's instructions (Invitrogen). Empty pMCS-GLuc plasmid with or without pCMV-Myc-*Bcl11a-XL* was transfected as a control. pCMV-SEAP (secreted alkaline phosphatase) was co-transfected in each well as a transfection control. Supernatant from

transfected cells was analyzed 48 hr after transfection. Luciferase assays were performed using the Secreted Pair Dual Luminesence Assay Kit (Genecopoeia) in accordance with the manufacturer's instructions and GloMax microplate luminometer (Promega). The values are reported as the mean ratio of luminescence intensity (RLU) of Gluc over SEAP. Values were collected from three independent experiments performed with at least three replicates per experiment.

Cell Culture and Western Blot

HEK293 cells were grown in DMEM supplemented with 10% fetal calf serum and 1% penicillin/streptomycin at 37°C under 5% CO_2 atmosphere. Cells were transfected using Lipofectamine 2000 in accordance with the manufacturer's instructions (Invitrogen). Total proteins were extracted with 1% Nonidet P-40 buffer in the presence of protease inhibitors (Roche), separated with SDS-PAGE, and electrophoretically transferred onto polyvinylidene fluoride membranes (Amersham). Membranes were blocked with 5% non-fat milk for 1 hr and incubated with rat anti-Sema3c (R&D Systems, Cat# MAB1728, RRID: AB_2301533) and mouse anti-beta-Actin (Abcam, Cat# ab8226, RRID: AB_306371) antibodies overnight, followed by treatment with horseradish peroxidase-conjugated secondary antibodies (Jackson ImmunoResearch) and ECL Plus western blotting detection reagents in accordance with the manufacturer's instructions (ThermoScientific).

Anterograde and Retrograde DiI Labeling

Brains were dissected from control and *Bcl11a*|*Emx1* mutant pups at P0 and fixed in 4% PFA. For anterograde labeling of the corticospinal and corticothalamic tracts, crystals of DiI (1,1'-dioctadecyl-3,3,3′,3′- tetramethylindocarbocyanine perchlorate; Molecular Probes) were inserted into the somatosensory and motor cortex region. For retrograde DiI labeling of corticospinal and corticothalamic neurons, DiI crystals were placed into the cerebral peduncle and thalamus, respectively. DiI-loaded tissues were incubated in the dark at 37°C for up to 21 days to permit dye diffusion. DiI tracings were examined on 100-μm-thick vibratome sections using a BX51 fluorescence microscope (Olympus).

Cell Counts and Statistical Analysis

For each experiment, at least three control and three mutant brains were analyzed, and three to five sections per brain were quantified. For in utero electroporation experiments, nuclear counterstaining with DAPI was used to distinguish between the VZ/SVZ, IZ, and CP. In some experiments IZ and CP were subdivided into equally sized bins as indicated in the respective figures. Stained cells were counted in radial units of 500-μm width in the presumptive somatosensory cortex of anatomically matched brain sections. For proliferation experiments, cells were counted in a radial unit of 250 μm. Caspase3 staining between P4 and P6 was evaluated in radial units of 1-mm width. Cells were counted using ImageJ (v1.48, RRID: nif-0000-30467) (NIH) and Photoshop CS4 (Adobe). Statistical analysis was done with Excel 2011 (Microsoft) or SPSS Statistic 21 (IBM) software. Significance between groups was assessed using a two-tailed Student's t test (or one-way ANOVA, followed by a least significant difference [LSD] post hoc test). p values < 0.05 were considered statistically significant.

ACCESSION NUMBERS

The accession number for the microarray data reported in this paper is GEO: GSE52827.

SUPPLEMENTAL INFORMATION

Supplemental Information includes Supplemental Experimental Procedures, eight figures, one table, and three movies and can be found with this article online at http://dx.doi.org/10.1016/j.neuron.2015.06.023.

AUTHOR CONTRIBUTIONS

C.W., R.S., S.S., V.T., and S.B. designed the experiments. C.W., K.P., C.K., R.S., M.S., J.C., and S.S. conducted the experiments and analyzed the data. P.L., N.A.J., and N.G.C. provided the *Bcl11a*^{flox} mice. C.W. and S.B. wrote the manuscript.

ACKNOWLEDGMENTS

We are grateful to C. Cepko (Harvard Medical School, Boston), F. Murakami (Osaka University), A. Nagy (Lunenfeld-Tanenbaum Research Institute, Toronto), K.-A. Nave (Max-Planck-Institute for Experimental Medicine, Göttingen), F. Polleux (Scripps Research Institute, La Jolla), and M. Vermeren (Babraham Institute, Cambridge) for the gift of mice and providing DNA plasmids. We thank S. Gässler for supporting the project and J. Andratschke, S. Takenaka, E. Werle, and F. Seigfried for excellent technical assistance. This work was supported by grants from the Deutsche Forschungsgemeinschaft (SFB 497/A9 and BR 2215 to S.B.; TA 303/6-1 to V.T.) and Ulm University (Bausteinprogramm 3.2 to C.W.). S.S. was supported by a Boehringer Ingelheim PhD fellowship. N.G.C. and N.A.J. were supported by the Cancer Prevention Research Institute of Texas (CPRIT) and are CPRIT Scholars in Cancer Research.

Received: February 4, 2014
Revised: May 4, 2015
Accepted: June 16, 2015
Published: July 15, 2015

REFERENCES

Alcamo, E.A., Chirivella, L., Dautzenberg, M., Dobreva, G., Fariñas, I., Grosschedl, R., and McConnell, S.K. (2008). Satb2 regulates callosal projection neuron identity in the developing cerebral cortex. Neuron *57*, 364–377.

Avram, D., Fields, A., Senawong, T., Topark-Ngarm, A., and Leid, M. (2002). COUP-TF (chicken ovalbumin upstream promoter transcription factor)-interacting protein 1 (CTIP1) is a sequence-specific DNA binding protein. Biochem. J. *368*, 555–563.

Bagnard, D., Lohrum, M., Uziel, D., Püschel, A.W., and Bolz, J. (1998). Semaphorins act as attractive and repulsive guidance signals during the development of cortical projections. Development *125*, 5043–5053.

Bagnard, D., Thomasset, N., Lohrum, M., Püschel, A.W., and Bolz, J. (2000). Spatial distributions of guidance molecules regulate chemorepulsion and chemoattraction of growth cones. J. Neurosci. *20*, 1030–1035.

Basak, A., Hancarova, M., Ulirsch, J.C., Balci, T.B., Trkova, M., Pelisek, M., Vlckova, M., Muzikova, K., Cermak, J., Trka, J., et al. (2015). BCL11A deletions result in fetal hemoglobin persistence and neurodevelopmental alterations. J. Clin. Invest. *125*, 2363–2368.

Britanova, O., de Juan Romero, C., Cheung, A., Kwan, K.Y., Schwark, M., Gyorgy, A., Vogel, T., Akopov, S., Mitkovski, M., Agoston, D., et al. (2008). Satb2 is a postmitotic determinant for upper-layer neuron specification in the neocortex. Neuron *57*, 378–392.

Chen, G., Sima, J., Jin, M., Wang, K.Y., Xue, X.J., Zheng, W., Ding, Y.Q., and Yuan, X.B. (2008). Semaphorin-3A guides radial migration of cortical neurons during development. Nat. Neurosci. *11*, 36–44.

Cooper, J.A. (2014). Molecules and mechanisms that regulate multipolar migration in the intermediate zone. Front. Cell. Neurosci. *8*, 386.

De Rubeis, S., He, X., Goldberg, A.P., Poultney, C.S., Samocha, K., Cicek, A.E., Kou, Y., Liu, L., Fromer, M., Walker, S., et al.; DDD Study; Homozygosity Mapping Collaborative for Autism; UK10K Consortium (2014). Synaptic, transcriptional and chromatin genes disrupted in autism. Nature *515*, 209–215.

Deciphering Developmental Disorders, S.; Deciphering Developmental Disorders Study (2015). Large-scale discovery of novel genetic causes of developmental disorders. Nature *519*, 223–228.

Evsyukova, I., Plestant, C., and Anton, E.S. (2013). Integrative mechanisms of oriented neuronal migration in the developing brain. Annu. Rev. Cell Dev. Biol. *29*, 299–353.

Feng, G., Mellor, R.H., Bernstein, M., Keller-Peck, C., Nguyen, Q.T., Wallace, M., Nerbonne, J.M., Lichtman, J.W., and Sanes, J.R. (2000). Imaging neuronal subsets in transgenic mice expressing multiple spectral variants of GFP. Neuron *28*, 41–51.

Flicek, P., Ahmed, I., Amode, M.R., Barrell, D., Beal, K., Brent, S., Carvalho-Silva, D., Clapham, P., Coates, G., Fairley, S., et al. (2013). Ensembl 2013. Nucleic Acids Res. *41*, D48–D55.

Goebbels, S., Bormuth, I., Bode, U., Hermanson, O., Schwab, M.H., and Nave, K.A. (2006). Genetic targeting of principal neurons in neocortex and hippocampus of NEX-Cre mice. Genesis *44*, 611–621.

Gorski, J.A., Talley, T., Qiu, M., Puelles, L., Rubenstein, J.L., and Jones, K.R. (2002). Cortical excitatory neurons and glia, but not GABAergic neurons, are produced in the Emx1-expressing lineage. J. Neurosci. *22*, 6309–6314.

Hancarova, M., Simandlova, M., Drabova, J., Mannik, K., Kurg, A., and Sedlacek, Z. (2013). A patient with de novo 0.45 Mb deletion of 2p16.1: the role of BCL11A, PAPOLG, REL, and FLJ16341 in the 2p15-p16.1 microdeletion syndrome. Am. J. Med. Genet. A. *161A*, 865–870.

Hatanaka, Y., Matsumoto, T., Yanagawa, Y., Fujisawa, H., Murakami, F., and Masu, M. (2009). Distinct roles of neuropilin 1 signaling for radial and tangential extension of callosal axons. J. Comp. Neurol. *514*, 215–225.

Hussman, J.P., Chung, R.H., Griswold, A.J., Jaworski, J.M., Salyakina, D., Ma, D., Konidari, I., Whitehead, P.L., Vance, J.M., Martin, E.R., et al. (2011). A noise-reduction GWAS analysis implicates altered regulation of neurite outgrowth and guidance in autism. Mol. Autism *2*, 1.

Iossifov, I., Ronemus, M., Levy, D., Wang, Z., Hakker, I., Rosenbaum, J., Yamrom, B., Lee, Y.H., Narzisi, G., Leotta, A., et al. (2012). De novo gene disruptions in children on the autistic spectrum. Neuron *74*, 285–299.

Ito, K., Kawasaki, T., Takashima, S., Matsuda, I., Aiba, A., and Hirata, T. (2008). Semaphorin 3F confines ventral tangential migration of lateral olfactory tract neurons onto the telencephalon surface. J. Neurosci. *28*, 4414–4422.

John, A., Brylka, H., Wiegreffe, C., Simon, R., Liu, P., Jüttner, R., Crenshaw, E.B., 3rd, Luyten, F.P., Jenkins, N.A., Copeland, N.G., et al. (2012). Bcl11a is required for neuronal morphogenesis and sensory circuit formation in dorsal spinal cord development. Development *139*, 1831–1841.

Jossin, Y., and Cooper, J.A. (2011). Reelin, Rap1 and N-cadherin orient the migration of multipolar neurons in the developing neocortex. Nat. Neurosci. *14*, 697–703.

Kwan, K.Y., Sestan, N., and Anton, E.S. (2012). Transcriptional co-regulation of neuronal migration and laminar identity in the neocortex. Development *139*, 1535–1546.

Leid, M., Ishmael, J.E., Avram, D., Shepherd, D., Fraulob, V., and Dollé, P. (2004). CTIP1 and CTIP2 are differentially expressed during mouse embryogenesis. Gene Expr. Patterns *4*, 733–739.

LoTurco, J.J., and Bai, J. (2006). The multipolar stage and disruptions in neuronal migration. Trends Neurosci. *29*, 407–413.

Luo, L. (2000). Rho GTPases in neuronal morphogenesis. Nat. Rev. Neurosci. *1*, 173–180.

Marín, O., Yaron, A., Bagri, A., Tessier-Lavigne, M., and Rubenstein, J.L. (2001). Sorting of striatal and cortical interneurons regulated by semaphorin-neuropilin interactions. Science *293*, 872–875.

Matsuda, T., and Cepko, C.L. (2007). Controlled expression of transgenes introduced by in vivo electroporation. Proc. Natl. Acad. Sci. USA *104*, 1027–1032.

Mattar, P., Langevin, L.M., Markham, K., Klenin, N., Shivji, S., Zinyk, D., and Schuurmans, C. (2008). Basic helix-loop-helix transcription factors cooperate to specify a cortical projection neuron identity. Mol. Cell. Biol. *28*, 1456–1469.

McEvilly, R.J., de Diaz, M.O., Schonemann, M.D., Hooshmand, F., and Rosenfeld, M.G. (2002). Transcriptional regulation of cortical neuron migration by POU domain factors. Science *295*, 1528–1532.

Miyoshi, G., and Fishell, G. (2012). Dynamic FoxG1 expression coordinates the integration of multipolar pyramidal neuron precursors into the cortical plate. Neuron *74*, 1045–1058.

Molyneaux, B.J., Arlotta, P., Menezes, J.R., and Macklis, J.D. (2007). Neuronal subtype specification in the cerebral cortex. Nat. Rev. Neurosci. *8*, 427–437.

Motoyama, N., Wang, F., Roth, K.A., Sawa, H., Nakayama, K., Nakayama, K., Negishi, I., Senju, S., Zhang, Q., Fujii, S., et al. (1995). Massive cell death of immature hematopoietic cells and neurons in Bcl-x-deficient mice. Science *267*, 1506–1510.

Namba, T., Kibe, Y., Funahashi, Y., Nakamuta, S., Takano, T., Ueno, T., Shimada, A., Kozawa, S., Okamoto, M., Shimoda, Y., et al. (2014). Pioneering axons regulate neuronal polarization in the developing cerebral cortex. Neuron *81*, 814–829.

Nieto, M., Monuki, E.S., Tang, H., Imitola, J., Haubst, N., Khoury, S.J., Cunningham, J., Gotz, M., and Walsh, C.A. (2004). Expression of Cux-1 and Cux-2 in the subventricular zone and upper layers II-IV of the cerebral cortex. J. Comp. Neurol. *479*, 168–180.

Niquille, M., Garel, S., Mann, F., Hornung, J.P., Otsmane, B., Chevalley, S., Parras, C., Guillemot, F., Gaspar, P., Yanagawa, Y., and Lebrand, C. (2009). Transient neuronal populations are required to guide callosal axons: a role for semaphorin 3C. PLoS Biol. *7*, e1000230.

Noctor, S.C., Martínez-Cerdeño, V., Ivic, L., and Kriegstein, A.R. (2004). Cortical neurons arise in symmetric and asymmetric division zones and migrate through specific phases. Nat. Neurosci. *7*, 136–144.

Ohshima, T., Hirasawa, M., Tabata, H., Mutoh, T., Adachi, T., Suzuki, H., Saruta, K., Iwasato, T., Itohara, S., Hashimoto, M., et al. (2007). Cdk5 is required for multipolar-to-bipolar transition during radial neuronal migration and proper dendrite development of pyramidal neurons in the cerebral cortex. Development *134*, 2273–2282.

Pacary, E., Heng, J., Azzarelli, R., Riou, P., Castro, D., Lebel-Potter, M., Parras, C., Bell, D.M., Ridley, A.J., Parsons, M., and Guillemot, F. (2011). Proneural transcription factors regulate different steps of cortical neuron migration through Rnd-mediated inhibition of RhoA signaling. Neuron *69*, 1069–1084.

Pasterkamp, R.J. (2012). Getting neural circuits into shape with semaphorins. Nat. Rev. Neurosci. *13*, 605–618.

Peter, B., Matsushita, M., Oda, K., and Raskind, W. (2014). De novo microdeletion of BCL11A is associated with severe speech sound disorder. Am. J. Med. Genet. A. *164A*, 2091–2096.

Piper, M., Plachez, C., Zalucki, O., Fothergill, T., Goudreau, G., Erzurumlu, R., Gu, C., and Richards, L.J. (2009). Neuropilin 1-Sema signaling regulates crossing of cingulate pioneering axons during development of the corpus callosum. Cereb. Cortex *19* (*Suppl 1*), i11–i21.

Polleux, F., and Ghosh, A. (2002). The slice overlay assay: a versatile tool to study the influence of extracellular signals on neuronal development. Sci. STKE *2002*, pl9.

Polleux, F., Morrow, T., and Ghosh, A. (2000). Semaphorin 3A is a chemoattractant for cortical apical dendrites. Nature *404*, 567–573.

Rajcan-Separovic, E., Harvard, C., Liu, X., McGillivray, B., Hall, J.G., Qiao, Y., Hurlburt, J., Hildebrand, J., Mickelson, E.C., Holden, J.J., and Lewis, M.E. (2007). Clinical and molecular cytogenetic characterisation of a newly recognised microdeletion syndrome involving 2p15-16.1. J. Med. Genet. *44*, 269–276.

Saito, T., and Nakatsuji, N. (2001). Efficient gene transfer into the embryonic mouse brain using in vivo electroporation. Dev. Biol. *240*, 237–246.

Sanno, H., Shen, X., Kuru, N., Bormuth, I., Bobsin, K., Gardner, H.A., Komljenovic, D., Tarabykin, V., Erzurumlu, R.S., and Tucker, K.L. (2010). Control of postnatal apoptosis in the neocortex by RhoA-subfamily GTPases determines neuronal density. J. Neurosci. *30*, 4221–4231.

Sasaki, S., Tabata, H., Tachikawa, K., and Nakajima, K. (2008). The cortical subventricular zone-specific molecule Svet1 is part of the nuclear RNA coded by the putative netrin receptor gene Unc5d and is expressed in multipolar migrating cells. Mol. Cell. Neurosci. *38*, 474–483.

Satterwhite, E., Sonoki, T., Willis, T.G., Harder, L., Nowak, R., Arriola, E.L., Liu, H., Price, H.P., Gesk, S., Steinemann, D., et al. (2001). The BCL11 gene family: involvement of BCL11A in lymphoid malignancies. Blood *98*, 3413–3420.

Schmittgen, T.D., and Livak, K.J. (2008). Analyzing real-time PCR data by the comparative C(T) method. Nat. Protoc. *3*, 1101–1108.

Schwenk, F., Baron, U., and Rajewsky, K. (1995). A cre-transgenic mouse strain for the ubiquitous deletion of loxP-flanked gene segments including deletion in germ cells. Nucleic Acids Res. *23*, 5080–5081.

Shelly, M., Cancedda, L., Lim, B.K., Popescu, A.T., Cheng, P.L., Gao, H., and Poo, M.M. (2011). Semaphorin3A regulates neuronal polarization by suppressing axon formation and promoting dendrite growth. Neuron *71*, 433–446.

Simon, R., Brylka, H., Schwegler, H., Venkataramanappa, S., Andratschke, J., Wiegreffe, C., Liu, P., Fuchs, E., Jenkins, N.A., Copeland, N.G., et al. (2012). A dual function of Bcl11b/Ctip2 in hippocampal neurogenesis. EMBO J. *31*, 2922–2936.

Srinivasan, K., Leone, D.P., Bateson, R.K., Dobreva, G., Kohwi, Y., Kohwi-Shigematsu, T., Grosschedl, R., and McConnell, S.K. (2012). A network of genetic repression and derepression specifies projection fates in the developing neocortex. Proc. Natl. Acad. Sci. USA *109*, 19071–19078.

Sugitani, Y., Nakai, S., Minowa, O., Nishi, M., Jishage, K., Kawano, H., Mori, K., Ogawa, M., and Noda, T. (2002). Brn-1 and Brn-2 share crucial roles in the production and positioning of mouse neocortical neurons. Genes Dev. *16*, 1760–1765.

Tabata, H., and Nakajima, K. (2003). Multipolar migration: the third mode of radial neuronal migration in the developing cerebral cortex. J. Neurosci. *23*, 9996–10001.

Tamamaki, N., Fujimori, K., Nojyo, Y., Kaneko, T., and Takauji, R. (2003). Evidence that Sema3A and Sema3F regulate the migration of GABAergic neurons in the developing neocortex. J. Comp. Neurol. *455*, 238–248.

Verhage, M., Maia, A.S., Plomp, J.J., Brussaard, A.B., Heeroma, J.H., Vermeer, H., Toonen, R.F., Hammer, R.E., van den Berg, T.K., Missler, M., et al. (2000). Synaptic assembly of the brain in the absence of neurotransmitter secretion. Science *287*, 864–869.

Yanagida, M., Miyoshi, R., Toyokuni, R., Zhu, Y., and Murakami, F. (2012). Dynamics of the leading process, nucleus, and Golgi apparatus of migrating cortical interneurons in living mouse embryos. Proc. Natl. Acad. Sci. USA *109*, 16737–16742.

Yu, Y., Wang, J., Khaled, W., Burke, S., Li, P., Chen, X., Yang, W., Jenkins, N.A., Copeland, N.G., Zhang, S., and Liu, P. (2012). Bcl11a is essential for lymphoid development and negatively regulates p53. J. Exp. Med. *209*, 2467–2483.

Zaidi, A.U., D'Sa-Eipper, C., Brenner, J., Kuida, K., Zheng, T.S., Flavell, R.A., Rakic, P., and Roth, K.A. (2001). Bcl-X(L)-caspase-9 interactions in the developing nervous system: evidence for multiple death pathways. J. Neurosci. *21*, 169–175.